bioRxiv preprint doi: https://doi.org/10.1101/2022.04.26.489587; this version posted April 28, 2022. The copyright holder for this preprint (which was not certified by peer review) is the author/funder. All rights reserved. No reuse allowed without permission.

ULTRASTRUCTURAL ANALYSIS OF CRF-DA INTERACTIONS IN MALE AND FEMALE MACAQUE: BEYOND THE CLASSIC VTA

E.A. Kelly[1], J.L. Fudge [1,2]

Departments of Neuroscience[1] and Psychiatry[2], University of Rochester School of Medicine and Dentistry, Del Monte Institute of Neuroscience, Rochester NY

Abbreviated title: CRF modulation of DA cell signaling

Corresponding Author: Julie L. Fudge, Del Monte Institute of Neuroscience, University of Rochester School of Medicine and Dentistry, 601 Elmwood Ave., Rochester NY 14642.
Julie_Fudge@urmc.rochester.edu
julie_fudge@urmc.rochester.edu
585-275-4535

ACKNOWLEDGEMENTS

We'd like to thank the URMC Electron Microscope Research Core for their expert guidance and assistance, Nanette Alcock (University of Rochester SMD) for histological preparations, Amita Kapoor (The Wisconsin National Primate Research Center, University of Wisconsin-Madison) for hormone assay processing (P51OD011106). This work was supported by the National Institutes of Mental Health (RO1MH115016 to J.L.F.)

bioRxiv preprint doi: https://doi.org/10.1101/2022.04.26.489587; this version posted April 28, 2022. The copyright holder for this preprint (which was not certified by peer review) is the author/funder. All rights reserved. No reuse allowed without permission.

ABSTRACT (250 words)

Dopamine (DA) is involved in stress and stress-related illnesses, including many psychiatric disorders. Corticotropin-releasing factor (CRF) plays a role in stress responses and targets the ventral midbrain DA system. This system is comprised of DA and non-DA cells and is divided into specific subregions. Although CRF inputs to the midline A10 nuclei of the DA system are well studied in rodents, in monkeys, CRF-containing terminals are highly enriched in the expanded A10 parabrachial pigmented nucleus (PBP) and in the A8 subregion (retrorubral field). In primates, the central extended amygdala, a rich source of CRF afferents across species, preferentially targets the PBP and A8 fields. We thus sought to characterize CRF terminals on DA (tyrosine hydroxylase, TH+) and non-DA (TH-) cell types in the PBP and A8 regions at the ultrastructural level using immuno-reactive electron microscopy (EM) for TH and CRF in male and female macaques. CRF labeling was present mostly in axon terminals, which mainly contacted non-DA dendrites in both subregions. Most CRF-positive terminals had inhibitory (symmetric) profiles. In the A8, CRF symmetric (inhibitory) contacts onto non-DA neurons were significantly greater than symmetric (excitatory) profiles; this pattern was also seen in the PBP, but did not reach statistical significance. No sex differences were found. Hormonal assays suggested that our animals were at similar developmental stages and experienced similar stress levels. Together our findings suggest that at baseline, CRF terminals in the primate PBP and A8 largely regulate DA indirectly through non-DA neurons.

KEYWORDS

corticotropin, dopamine, non-human primate, electron microscopy

KEY POINTS (3 max)

- In addition to midline A10 neurons, CRF terminals robustly target the enlarged A10 PBP and A8 regions in primate ventral midbrain
- CRF terminals in the Macaque PBP/A8 mainly contact non-DA neurons compared to DA neurons
- Relatively more CRF-positive terminals are symmetric (inhibitory) versus asymmetric (excitatory) in both PBP and A8, suggesting indirect, possibly interneuronal, mechanisms of DA control.

bioRxiv preprint doi: https://doi.org/10.1101/2022.04.26.489587; this version posted April 28, 2022. The copyright holder for this preprint (which was not certified by peer review) is the author/funder. All rights reserved. No reuse allowed without permission.

INTRODUCTION

The monoamine neurotransmitter, dopamine (DA) is important in many fundamental behaviors including positive and negative reinforcement, decision making, working memory, incentive and stimulus salience and purposeful movement. There are 12 DA neuron clusters throughout the brain, however the majority of DA neurons are located in three anatomical groups in the ventral midbrain, namely the ventral tegmental area (VTA, A10), the substantia nigra pars compacta (SNc, A9) and the retrorubral field (RRF, A8; Pearson et al., 1983; Arsenault et al., 1988; Bjorklund and Dunnett, 2007; Watabe-Uchida et al., 2012; Beier et al., 2015; Morales and Margolis, 2017). In primates, the lateral part of the VTA, the parabrachial pigmented nucleus (PBP, A10), extends from the midline VTA (A10), to stretch dorsally across the mediolateral extent of the ventral midbrain, and transitions caudally into the RRF (A8; Halliday and Tork, 1986; Fudge et al., 2017). The PBP and A8 are disproportionately expanded territories in nonhuman and human primate, compared to other regions (Halliday and Tork, 1986; McRitchie et al., 1996; Francois et al., 1999; Fu et al., 2016). The DA subregions are composed of cells with diverse phenotypic characteristics, and are differentially connected with various brain areas correlating with their anatomic position in the ventral midbrain (Haber et al., 2000; Arias-Carrion et al., 2010; Lammel et al., 2011; Lammel et al., 2014; Farassat et al., 2019). As one example of cellular heterogeneity across subregions, we recently found a broad range of DA-to-GABAergic neuron ratios in different subregions in monkey, suggesting differences in intrinsic control of DA firing (Kelly et al. 2022, *under review*).

In rodents, the best-studied animal model, the DA neurons receive excitatory, inhibitory, and modulatory input from diverse sources (Lewis and Sesack, 1997; Watabe-Uchida et al., 2012; Morales and Margolis, 2017). Corticotropin-releasing factor (CRF) is found in some of these afferent sources, and is a neuromodulator of DA cell firing, although the precise mechanism is not understood (Kalivas et al., 1987; Ungless et al., 2003; Orozco-Cabal et al., 2006; Gallagher et al., 2008; Wanat et al., 2008; Wanat et al., 2013; Grieder et al., 2014). Potential sources of CRF to the various DA subregions are therefore diverse, but have not been well studied (reviewed in, Kelly and Fudge, 2018). A large known source of CRF to the rodent and primate PBP and A8 subregions arises from the central extended amygdala (Rodaros et al., 2007; Dabrowska et al., 2016; Fudge et al., 2017).

In rodents, the ventral tegmental area (VTA) is seen as an important effector site for CRF action, due to its outputs to the ventral striatum and medial prefrontal cortex in that species (reviewed in, Bjorklund and Dunnett, 2007; Morales and Margolis, 2017). In primates, evolutionary extension of the ventral midbrain

bioRxiv preprint doi: https://doi.org/10.1101/2022.04.26.489587; this version posted April 28, 2022. The copyright holder for this preprint (which was not certified by peer review) is the author/funder. All rights reserved. No reuse allowed without permission.

results in differential expansions of VTA subnuclei (A10), the A9, and A8 regions. With this expansion, the pattern of efferent and afferent circuits through these areas also shifts (reviewed in, Bjorklund and Dunnett, 2007; Cho and Fudge, 2010; Fudge et al., 2017). It is now recognized that the broad expanse of the primate DA system is physiologically heterogeneous across the mediolateral axis with respect to both intrinsic firing, and coding properties. DA neurons in the 'midline' VTA nuclei code reward prediction errors (Mirenowicz and Schultz, 1994; Tobler et al., 2003), while more dorsolaterally placed DA neurons in the vicinity of the PBP and A8, are 'salience' coding, i.e. respond to potentially salient stimuli regardless of value (Matsumoto and Hikosaka, 2009; Bromberg-Martin et al., 2010). These differences suggest that CRF terminals in the 'midline' VTA versus PBP/A8 subpopulations may have differing functional roles, since each region forms specific circuits (Haber et al., 2000; Bromberg-Martin et al., 2010; Fudge et al., 2017). The organization of CRF terminals in DA subpopulations outside of the classic VTA --i.e. in regions associated with 'salience' coding of noxious and novel stimuli--is of interest.

In this study, we investigated the interactions of CRF-positive terminals in the PBP and A8 subregions in young male and female macaques. Using dual immuno-peroxidase reactivity for electron microscopy (EM), we quantified ultrastructural synaptic contacts of CRF-reactive fibers onto either tyrosine hydroxylase (TH) positive ('DA'), and TH-negative ('non-DA') neurons in the PBP and A8 subregions.

MATERIAL AND METHODS

Animals.

All experiments were conducted in accordance with National Institute of Health guidelines (NIH Publications No. 80-23). Experimental design and technique were aimed at minimizing animal use and suffering and were reviewed by the University of Rochester Committee on Animal Research. Animals were all socially housed by sex. To conserve animals, we used perfused tissue from 3 young male and 3 young female monkeys (*Macaque fascicularis*) that had received tracer injections in other brain regions as part of other studies (**Table 1**).

Histology.

All animals were sacrificed under deep anesthesia (pentobarbital) by intracardiac perfusion, first with 0.9% sterile saline and then 6L of 4% paraformaldehyde (PFA) in a solution of sucrose and phosphate buffer (PB, pH 7.4). Brains were harvested and placed in 4% PFA overnight, and then sunk in increasing gradients of sucrose solution (10%, 20% and 30%). The entire brain was coronally sectioned on a freezing sliding microtome at 40 um and all sections were saved in serial wells (24 serial ‘compartments’; 1:24) in a cold cryoprotectant solution containing 30% sucrose and 30% ethylene glycol in PB at -20°.

bioRxiv preprint doi: https://doi.org/10.1101/2022.04.26.489587; this version posted April 28, 2022. The copyright holder for this preprint (which was not certified by peer review) is the author/funder. All rights reserved. No reuse allowed without permission.

Antibody Characterization

The antibodies used in this study are well documented and detailed in **Table 2**. Anti-CRF (rabbit, T-4037, Peninsula) shows specific localization of CRF in axon terminals (Tagliaferro and Morales, 2008; Fudge et al., 2017; Kelly and Fudge, 2018; Yuan et al., 2019) and has been thoroughly tested using pre-absorption assays (JCN antibody database ID #AB-518252). In primate, we have previously shown specific immunoreactivity in CRF positive cells and fibers throughout the macaque brain (Fudge et al., 2017; Kelly and Fudge, 2018), with similar findings as reports using other CRF antibodies (Cha and Foote; Bassett and Foote). Anti-tyrosine hydroxylase (TH, mouse, MAB518, Millipore, clone LNC1) is well documented in many species (JCN antibody database ID # AB-2201528) and shows reactivity in DA neurons of the ventral midbrain with little to no background immunoreactivity throughout (Cho and Fudge, 2010). Our results are in agreement with previously reported distribution and cytoarchitecture of dopaminergic cells in monkey (Arsenault et al., 1988). TH-immunoreactivity in the ventral midbrain has long been an accepted marker of dopaminergic cells in the ventral midbrain, since there is no staining for enzymes involved in the synthesis of norepinephrine or epinephrine in this region (Gaspar et al., 1983; Pearson et al., 1983). The pattern of calbindin-D28K (CaBP) expression is also identical to published reports for primate A10 and A8 dopamine neurons (Cote et al., 1991; Gaspar et al., 1993; McRitchie et al., 1996), and is authenticated in several species (JCN antibody database ID #AB-476894).

Single Immunocytochemistry.

For precise region of interest (ROI) determination in electron microscopy preparations, neighboring compartments of tissue were singly immunoreacted for anti-Calbindin D28k (CaBP,a marker of the A10 and A8 DA subpopulation 1:10K, Sigma #C9848, mouse,Haber and Fudge, 1997), anti-CRF (1:1K, Penisula #T-4037, rabbit) and anti-tyrosine hydroxylase (TH, a marker for DA neurons and processes, 1:10K, Millipore #MAB318, mouse). Briefly, sections were rinsed thoroughly in 0.1M phosphate buffer (PB, pH 7.4) containing 0.3% Triton-X (TX) followed by an endogenous peroxidase step (10% methanol, 3% H_2O_2 in 0.1M PB). Sections were then rinsed thoroughly in PB-TX and blocked with 10% normal goat serum in PB-TX (NGS-PB-TX; primary antisera). Following rinses in PB-TX, tissues were incubated in primary antisera for ~96 hours at 4°C. Tissues were then rinsed with PB-TX, blocked with 10% NGS-PB-TX, incubated in the appropriate biotinylated secondary antibody (goat anti-rabbit, #BA-100; goat anti-mouse, Vector Labs #BA-9200;Vector Laboratories, Burlington, ON Canada) and then incubated with avidin-biotin complex (Vectastain ABC kit, PK-6100 [ABC Elite, for CaBP and TH] or PK-4000 [Standard ABC kit, for CRF], Vector Laboratories, Burlington, ON Canada). After rinsing, sections were visualized with 2,2'-diaminobenzidine (DAB, 0.05mg/ml, 0.3% H_2O_2, in 0.1M Tris-buffer), and rinsed thoroughly prior to mounting. Sections were mounted out of mounting solution (0.5% gelatin in 20% ETOH in double distilled water) onto subbed slides, dried for 3 days, and cover slipped with DPX mounting media (Electron Microscopy Sciences).

bioRxiv preprint doi: https://doi.org/10.1101/2022.04.26.489587; this version posted April 28, 2022. The copyright holder for this preprint (which was not certified by peer review) is the author/funder. All rights reserved. No reuse allowed without permission.

Double-immunoperoxidase and immunogold-reactivity for CRF and TH (EM).

We quantified ultrastructural proximity of CRF positive fibers and TH positive cells. Adjacent brain sections were dually stained for CRF-IR and TH-IR (Figure 2 , Kelly et al., 2014). Briefly, sections were washed thoroughly in freshly-made filtered 0.05M phosphate buffered saline (PBS), subjected to antigen retrieval (1% sodium borohydride in 0.1M filtered 0.1M PB), and blocked in a solution containing 3% NGS and 1% bovine serum albumin (BSA). Sections were incubated for 24-hours in the same blocking solution with rabbit anti- CRF (Penisula,T-4037, 1:2K) and mouse anti-TH (Millipore, MAB318, 1:5K) at 4°C on a shaker followed by 24-hours at room temperature (RT). Sections were then washed in filtered 0.05M PBS and incubated for 4 hours in goat anti-rabbit IgG conjugated to biotin (1:200, Jackson ImmunoResearch, BA-1000), followed by ABC (per product instructions; Elite ABC Kit, Vector Labs, PK-6100). CRF immuno-reactivity was visualized with 3,3'-diaminobenzidine (0.5mg/ml; DAB) and hydrogen peroxide (0.03%) in 0.1M PB. Sections were rinsed thoroughly in filtered 0.05M PBS, followed by a second pre-incubation in a washing buffer solution containing 3% NGS, 0.8% BSA, 0.1% cold water fish gelatin in 0.1M PBS. Sections were then incubated for 24 hours in goat-anti-mouse immunogold (Nanogold, N2915, Nanoprobes Inc., Yaphank, NY) in washing buffer at RT on a shaker. Following a thorough wash, tissue was incubated in 2.5% glutaraldehyde for 10 minutes at RT. Sections were rinsed thoroughly in 0.1M PBS, followed by a series of washes in Enhancement Conditioning Solution (1X concentration per package instructions, Electron Microscopy Science [EMS], Cat 25830, Hatfield PA). Sections were silver enhanced using the Aurion R-Gent SE-EM Kit (EMS, Cat #25520-90). Following additional post-fixation in 1% osmium tetroxide (EMS, Cat #19150), sections were dehydrated in ascending concentrations of ethanol. Sections were then treated with propylene oxide, impregnated in resin (Embed 812, Araldite 502, DDSA, DMP-30 [all EMS]) overnight at RT, mounted between ACLAR embedding films (EMS, Cat# 50425) and cured at 55°C for 48-hours. The PBP and A8 regions were excised in a trapezoid shape (to determine anatomical orientation) from the embedding films and re-embedded at the tip of resin blocks. Ultrathin sections (60-80 nm; evidenced by the sections silver sheen) were cut with an ultramicrotome (Reichert Ultracut E) and collected in sequence on bare square-mesh nickel grids (EMS, G200-Ni).

EM Imaging and Data Analysis.

Eighty electron micrographs were randomly taken at 30,000X in rostral and caudal midbrain (approximately 10 microns from the resin margin) in each animal corresponding to a total surface of ~ 1,000 μm^2 of neuropil per animal (as in, Tremblay et al., 2007; Bouvier et al., 2008; Kelly et al., 2014). Images were captured on a Hitachi 7650 Transmission Electron Microscope using a Gatan 11-megapixel Erlangshen digital camera and Digital Micrograph software. TIFF images were exported into Adobe Photoshop and Adobe Illustrator (v2022) and adjusted for brightness and contrast in preparation for analysis. Cellular profiles were identified using a series of criteria previously defined in single-ultrathin sections (Peters et al., 1991; Kelly et al., 2014). In instances when immuno-reactive density obscured some of the intracellular organelles and defining characteristics, we relied on the visible defining features, such as contours made

bioRxiv preprint doi: https://doi.org/10.1101/2022.04.26.489587; this version posted April 28, 2022. The copyright holder for this preprint (which was not certified by peer review) is the author/funder. All rights reserved. No reuse allowed without permission.

by the profiles and ultrastructural relationships with neighboring elements to aid in our classification. The following classifications were applied to characterize labeled elements (primarily dendrites and axonal terminals in this study), and also surrounding neuropil to assess the nature of CRF-terminal contacts onto non-TH labeled structures.

Axon terminal- Axonal terminals were distinguished from other subcellular profiles based primarily on the presence of synaptic vesicles, with rounded to elongated morphologies, but also of synaptic contacts with dendritic shafts and spines. Axon terminals generally contained mitochondria.

Dendrite- Dendritic shafts cut longitudinally were recognized by their irregular contours, elongated mitochondria in parallel with their central axis, frequent protuberances (spines, filopodia, small branches), and synaptic contacts with axon terminals. When cut transversally, dendritic shafts were identified by their rounded morphology, frequent occurrence of mitochondria and microtubules, and they were distinguished from unmyelinated axons by their larger diameter.

Glia- Protoplastic astrocytes were recognized as electron-lucent structures seen to encase and wrap around other neuropil structures. As a result, astrocytes maintained irregular and angular shapes, distinguishing them from other neuronal profiles having a characteristic rounded shape. Microglia processes displayed irregular contours with obtuse angles, distinctive long stretches of endoplasmic reticulum, numerous large vesicles, occasional multi-vesicular bodies, vacuoles or cellular inclusions, and distinctive surrounding extracellular space.

Dendritic Spines- Dendritic spines cut longitudinally often protruded from dendritic shafts, displayed rounded morphologies and were free of mitochondria. Spines were characterized primarily by the presence of electron-dense accumulations (postsynaptic densities) at synaptic contact sites with axons.

Quantitative Analysis.

We define "contacts" as CRF-IR axon terminals that make either symmetrical or asymmetrical synaptic profiles with a post-synaptic element. “Close contacts”, where the presynaptic membrane came close but did not touch the postsynaptic cell, were not counted. To quantify symmetrical (inhibitory) vs. asymmetrical (excitatory)-type synapses, the number of synaptic contacts was counted in an area of 1,000 μm^2 total neuropil per animal from approximately 80 electron micrographs per animal per midbrain region. In each micrograph, a CRF-labeled axon terminal was determined (see classification above) and synapse contact type were determined based on both the physical abutment of the presynaptic membrane with that of the postsynaptic cell and the appearance of a thick or thin postsynaptic density (asymmetric vs symmetric respectively). The total number of asymmetric and symmetric contacts were calculated for each case. We then determined the cell type that each CRF positive axon made contact with based on the appearance of immunogold labeling in the postsynaptic cell (i.e. TH positive). We quantified (1) the total number of DA positive and non-DA positive cells receiving a synaptic contact from a CRF positive axon terminal, (2) the proportion of asymmetric vs symmetric contacts across all cell types in the PBP versus A8, and (3) the proportion of asymmetric and symmetric contacts onto either DA positive or non-DA positive cells in each

bioRxiv preprint doi: https://doi.org/10.1101/2022.04.26.489587; this version posted April 28, 2022. The copyright holder for this preprint (which was not certified by peer review) is the author/funder. All rights reserved. No reuse allowed without permission.

region. Proportions were determined (1) dividing the number of asymmetric or symmetric contacts by the total number of contacts and (2) by dividing the total number of each synapse type by the total number of each cell type.

Hormone Assays

To assess the stability of pubertal and stress measures in our male and female animals under usual conditions (pair housing) maintained in our facility, serum specimens were collected and assayed on 7 animals (n= 3 males, n=4 females) kept in our facility in 2020. Four animals were used in the current study. The objective was to determine the general variability in gonadal steroids and cortisol over time in pair-housed animals of similar age. Assays were run at the Wisconsin National Primate Research Center, under the supervision of Dr. Amita Kapoor. The following references provide a detailed report of the techniques used for these analyses: Multi-steroid Assays from Serum: (Kenealy et al., 2016) and radioimmunoassay for lutenizing hormone (Garcia et al., 2018). Specimens were collected at three time points throughout the study: 1) when animals were released from quarantine [60 days after arrival to the facility], 2) just before tract-tracer surgery [approximately 30-90 days after release from quarantine] and 3) on the morning of sacrifice (approximately 2 weeks after surgery). Thus, three samples per animal were collected over an approximate 6-month period. All samples were collected at the University of Rochester and shipped on dry ice for hormone analysis off-site. At least 2 mL of serum (from 4mL whole blood) was collected using either an IV catheter or butterfly needle/syringe into red topped tubes. Blood was then centrifuged, and serum pipetted off and stored at -20 until shipped.

Statistics.

Analysis was performed with Prism 9 software (GraphPad Software). All values reported in the text are mean ± standard error of the mean (SEM). For all statistical tests, significance was set to $p<0.05$. Multiple group comparisons (cell type vs synapse profile, **Figures 4** [pooled comparisons], **Figure 5** [male/female comparisons]) were analyzed using a Two-way ANOVA with corrected Tukey's multiple comparisons post-hoc tests. Sample size (n) represents individual animals.

RESULTS

Delineation of the PBP and A8 subpopulations. The A10 neurons in the nonhuman primate extend the entire rostrocaudal extent of the midbrain (approximately 6 mm), and include the following subnuclei: the rostral linear nucleus (RLi), the caudolinear nucleus (CLi), the intrafascicular nucleus, the ventral tegmental nucleus (VTA), the paranigral nucleus, and the parabrachial pigmented nucleus (PBP, Halliday and Tork, 1986; McRitchie et al., 1995). In human and in monkey, the PBP is by far the largest sub-nucleus of the A10 (Halliday and Tork, 1986; Olszewski and Baxter, 2014), and sweeps dorsolaterally over the entire A9 region, to merge caudally with the A8 group. We therefore grouped all individual VTA subnuclei medial to the PBP as the 'midline VTA' group, and designated the PBP as a separate A10

bioRxiv preprint doi: https://doi.org/10.1101/2022.04.26.489587; this version posted April 28, 2022. The copyright holder for this preprint (which was not certified by peer review) is the author/funder. All rights reserved. No reuse allowed without permission.

subnucleus. PBP TH-positive neurons are frequently larger than other A10 neurons, and oriented horizontally with long proximal dendrites in the mediolateral plane.

CaBP immunoreactivity is a reliable marker used for the determination of the A10 and A8 DA subregions across species (Lavoie and Parent, 1991; Gaspar et al., 1993; McRitchie et al., 1996; Haber and Fudge, 1997), due to high expression in many A10 and A8 DA cells, and a noticeable absence in the SNc (A9) DA cells (**Figure 1A**, rostrocentral, **1D**, caudal). Large fiber paths (i.e. the oculomotor bundle, III, and medial lemniscus, ml) also remain unstained and serve as additional landmarks for subregional boundaries. By comparing the distribution of CRF-positive terminals with adjacent CaBP-labeled sections, robust CRF innervation was found predominately at rostrocentral levels over the PBP, and at caudal levels over the RRF/A8 region (Figure 1D [rostrocentral], 1E [caudal]; Kelly and Fudge, 2018). There were few labeled fibers extending into the CaBP-negative A9 region (**Figure 1C**, **F**). As expected, CRF-positive axonal terminals were also found in the midline VTA nuclei which was higher at rostrocentral compared to caudal levels. In both the PBP and A8, dense patches of CRF-labeled fibers consisted of very thin, highly varicose fibers, as well as slightly thicker, beaded 'fibers en passant', seen under higher magnification (PBP, **Figure 1C;** RRF /A8, **Figure 1F**) .

For region of interest (ROI) localization in EM studies, adjacent sections were immunostained for CRF, TH (a marker for DA in the ventral midbrain; Pearson et al., 1983) and CaBP (**Figure 2**). This approach allowed us to sample from areas with known dense termination of CRF positive fibers specifically in the PBP or A8, confirmed by matching microscopic anatomical landmarks (blood vessels patterns) for accurate excision of PBP and A8 blocks for EM samples.

Characteristics of CRF-labeled axon terminals

At the EM level, CRF immunoreactivity was predominantly found in axon terminals (**Figure. 3**) and some dendrites (not shown). Depending on the plane of sectioning, CRF positive axon terminals presented as small spherical elements (cross sections) or elongated (oblique or longitudinal sections) deposits of granular material. CRF positive axon terminals made contacts (defined as either asymmetric or symmetric type terminal appositions) onto both TH- positive (DA) and TH-negative (non-DA) dendrites.

TH immunoreactivity was visualized using gold/silver enhancement (**Figure 3**) which results in small electron dense deposits spaced throughout the cellular element, mainly in dendritic structures. Importantly, the gold labeling protocol was titrated so as to not obstruct classification of synaptic contacts, permitting visualization of large post-synaptic densities (PSDs) that suggest asymmetric (excitatory, black arrow heads) synapses, versus the thin PSDs that make up symmetric (inhibitory, white arrow heads) contacts. The majority of TH immunoreactivity was in large dendritic structures, characterized by an electron lucent cytoplasm, multiple mitochondria, and PSDs at points of excitatory contacts (**Figure 3A-G,** excitatory

bioRxiv preprint doi: https://doi.org/10.1101/2022.04.26.489587; this version posted April 28, 2022. The copyright holder for this preprint (which was not certified by peer review) is the author/funder. All rights reserved. No reuse allowed without permission.

contacts= black arrowheads, **Figure 4A,** pink). Single TH-positive dendrites often displayed multiple synaptic contacts, both symmetric and asymmetric in nature. Asymmetric contacts are discernable by an obvious protein accumulation on the side of the postsynaptic compartment (PSD) with a thickness of 25-50 nanometers (**Figure 3, 4A** black arrowheads). In contrast, CRF symmetric contacts (inhibitory) have a slight electron-dense thickening associated with the postsynaptic membrane and are classified by the abutment of pre- and postsynaptic membranes with an absence of PSD accumulation (**Figure 3,4A,** white arrowheads). Non-TH immunoreactive dendrites were identified as having similar ultrastructural features, but without silver particles (Fig. 4A, yellow).

CRF contacts onto non-DA cells predominate in both PBP and A8

We first quantified CRF contacts on each cell type in the PBP and A8 (**Figure 4B**). We found that 89% of all contacts were onto non-DA cells in PBP and 86% of all contacts were onto non-DA cells in A8 (Two-way ANOVA, $F(1,14)=46.06$, $p<0001$; PBP, black bars (PBP), $p=0.0012$; white bars (A8), $p=0.0018$, Tukey's multiple comparisons test). Thus, the relative frequency of CRF contacts on DA versus non-DA cells was similar in the PBP and A8 (within DA comparisons: $p=0.9985$ n.s.; within non-DA comparisions: $p=0.9288$ n.s., two-way ANOVA with Tukey's multiple comparisons test).

The proportion of CRF inhibitory contacts is greater than excitatory contacts in PBP and A8

We next quantified the proportion of either asymmetric (excitatory) or symmetric (inhibitory) contacts across region (**Figure 4C**). In the PBP and A8, symmetric contacts comprised the majority of contacts (62% in the PBP, black bars, $p=0.0036$, Tukey's multiple comparisons test; 63% in the A8, A8, white bars, $p=0.0007$, Tukey's multiple comparisons test). Here we found a significant interaction in synapse type (asymmetric vs symmetric, two-way ANOVA, $F(1,14)=44.69$, $p<0.0001$) denoted by the disproportionate number of symmetric contacts. The number of asymmetric contacts that was similar across regions (PBP vs A8, two-way ANOVA, $F(1,14)=0.012$, $p=0.9146$ n.s.). These data suggest that CRF-mediated regulation of inhibitory versus excitatory contacts is similar in PBP and A8.

Characterizing type of CRF contact onto DA and non-DA cells types in the PBP and A8

We next investigated the nature of CRF interactions in the PBP versus A8 subregions, by quantifying the proportion of CRF-positive axon contacts across both cell type (DA vs non-DA) as well as synapse type (asymmetric [+] vs symmetric [-]). In the PBP (**Figure 4D**), we found that 89% of asymmetric contacts (black bars) were found on non-DA cells ($p=0.0002$, two way-ANOVA with Tukey's multiple comparisons tests). Similarly, 85% of symmetric contacts (gray bars) were also found on non-DA cells ($p<0.0001$, Tukey's multiple comparisons test). Thus, there were significantly more synaptic contacts overall onto non-DA cells compared to DA positive cells (significant effect across cell type [DA versus non-DA], two-way ANOVA, $F(1,12)= 103.7$, $p<0.0001$). However, the proportion of symmetric vs asymmetric contacts did not differ within each cell group (two-way ANOVA, $F(1,12)=4.114$, $p=0.06$).

bioRxiv preprint doi: https://doi.org/10.1101/2022.04.26.489587; this version posted April 28, 2022. The copyright holder for this preprint (which was not certified by peer review) is the author/funder. All rights reserved. No reuse allowed without permission.

In the RRF/A8 (**Figure 4E**), we similarly found significantly more synaptic contacts onto non-DA positive cells compared to DA positive cells. We performed a two-way ANOVA to assess the effect of cell type (DA vs non-DA) and synapse type (symmetrical vs asymmetrical) on the proportion of CRF positive axon contacts and found a significant interaction [$F(1,16)=11.82$, $p=0.0034$] for both cell types [$F(1,16)=129$, $p<0.0001$] and synapse types [$F(1,16)=16.95$, $p=0.0008$]. Within the asymmetric contacts (black bars), we found that 85% of those contacts were onto non-DA cells ($p=0.0002$; Tukey's multiple comparisons test). Among the symmetric contacts (gray bars), we found that 88% of those contacts were also onto non-DA cells (white bars, $p<0.0001$, Tukey's multiple comparisons test). We next analyzed differences in the proportion of asymmetric versus symmetric contacts across post-synaptic cell types (DA vs non-DA). Non-DA cells had significantly greater proportions of symmetric (inhibitory) type synapses compared to excitatory type synapses ($p=0.0003$, Tukey's multiple comparisons test). The proportion of asymmetric vs symmetric contacts in the DA cell population was not significantly different from one another ($p=0.9625$, Tukey's multiple comparisons test).

Frequency of CRF-positive axon contacts are comparable across males and females

CRF is differentially regulated in males and females via several mechanisms (Bangasser and Valentino, 2012; Bangasser et al., 2013). In females, stress induces enhanced CRF-mediated activation of the HPA axis and has enhanced effects on post-synaptic receptor dynamics (reviewed in, Bangasser and Valentino, 2012). To compare potential sex differences in the frequency of CRF-positive terminal interactions onto DA or non-DA neurons in the PBP and A8, we compared CRF-positive synaptic contacts across cell type in males and females (**Figure 5A**). Similar to pooled cases (**Figure 4**), we noted significantly more contacts made on non-DA cells in males, with 93% of all contacts on non-DA cells in the PBP and 86% of all contacts on non-DA cells in A8. This was confirmed following statistical analysis (PBP, solid blue bar, $p=0.0084$; A8, hatched blue bar, $p=0.05$; Tukey's multiple comparisons) with a significant effect for cell type (two-way ANOVA, $F(1,10)=51.93$, $p<0.0001$). In females, 83% and 91% of all contacts were on non-DA cells in PBP and A8 respectively, however, significance was not seen across the two cell types (solid red bar vs hatched red bar). CRF contacts in males and females were not significantly different within each DA population (DA, males vs females, PBP, $p=0.9999$; DA, males vs females, A8, $p=0.9987$; non-DA, males vs females, PBP, $p=0.3574$; non-DA, males vs females, A8, $p=0.9998$).

We next compared the proportion of synapse type (asymmetric and symmetric) across DA and non-DA neurons in males and females. In PBP (**Figure 5B**), there were more contacts made onto non-DA cells regardless of synapse type in males (solid blue vs hatched blue, 92% of all asymmetric contacts were onto non-DA cells, $p=0.0408$, 85% of all symmetric contacts were onto non-DA cells, $p=0.0134$) when compared to DA cells. In females, 85% of all asymmetric contacts were onto non-DA cells (solid red vs hatched red, non-DA asymmetric: $p=0.0491$) and 81% of all symmetric contacts were onto non-DA cells (solid red vs

bioRxiv preprint doi: https://doi.org/10.1101/2022.04.26.489587; this version posted April 28, 2022. The copyright holder for this preprint (which was not certified by peer review) is the author/funder. All rights reserved. No reuse allowed without permission.

hatched red, non-DA symmetric: p=0.0159). We did not find significant differences between sexes when comparing within synapse type (blue solid vs red solid; hatched blue vs hatched red, all comparisons p>0.9999). Given the disproportionate number of contacts onto non-DA cells in PBP, we further compared whether there were more asymmetric vs symmetric contacts within this subpopulation of cells. Here again, we did not find significant differences (males, blue hatched bars, p=0.9146; females, red hatched bars, p=0.78).

Similarly, in RRF/A8 (**Figure 5C**), we found 81% and 84% of all asymmetric and symmetric contacts, respectively, were on non-DA cells compared to DA cells in males. In across-cell type comparisons, males did not show a significant difference in the proportion of asymmetric contacts on DA vs non-DA cells (solid blue bar vs hatched blue bar, p=0.06). In contrast, significantly more symmetric contacts were made onto non-DA cells compared to DA cells in males (blue bar vs hatched blue, p=0.0002). Females showed a similar trend with 89% of all asymmetric contacts and 93% of all symmetric contacts on non-DA cells suggesting an overall prevalence for synaptic interaction on the non-DA population of cells. These differences were highly significant in the female cohort, as shown in across-cell type comparisons (female asymmetric synapses ,solid red bar vs hatched red bar, p=0.0172; female symmetric synapses, solid red bar vs hatched red bar, p=0.0002; Tukey's multiple comparisons test). To further assess the disproportionate number of contacts in non-DA cells in A8, we further compared whether there were more asymmetric vs symmetric contacts within this subpopulation of cells. We found significantly more symmetric synapses across both sexes in non-DA cells (males, blue comparison bar below graph, p=0.0171; females, red comparison bar below graph, p=0.0132). We did not see significant differences in males vs female proportions in RRF/A8.

It is interesting to note that while both DA subregions (PBP and A8) display a high proportion of contacts onto non-DA cells, the proportion of asymmetric vs symmetric contacts within each of these cell populations was similar in most comparisons. This was not the case when comparing the asymmetric vs symmetric proportions in the A8 non-DA cells. Here we found (in both pooled [**Figure 4**] and sex comparison data [**Figure 5**]) significantly more symmetric (inhibitory) contacts onto non-DA cells in A8. These differences could be explained by the ratio of DA vs non-DA neurons in these regions and its influence on our probability to record non-DA interactions in PBP (see Discussion). It might also suggest a unique CRF-mediated modulation within the A8 region.

CRF contacts are not influenced by sex or hormonal status in young macaques

How CRF expression and stress impact the DA system may be developmentally regulated (Coco et al., 1992; Izzo et al., 2005; Rincon-Cortes and Grace, 2017). Adolescent monkeys are transitioning into sexual maturation at three to five years of age, with changes in physical parameters (vaginal epithelial changes, testicular volume) as well as hormonal shifts (Plant, 2015). To determine if pubertal status or stress effects

bioRxiv preprint doi: https://doi.org/10.1101/2022.04.26.489587; this version posted April 28, 2022. The copyright holder for this preprint (which was not certified by peer review) is the author/funder. All rights reserved. No reuse allowed without permission.

was a factor in our cohort, we performed gonadal hormone and cortisol assays from serum specimens on seven animals (four of which are included in this study) at several timepoints (**Table 3**). In serum preparations, analyte concentrations were comparable between males and females with expected differences between gonadal hormones. Stress hormones were not significantly different from one another across animals (**Figure 6**). These findings suggest that overall developmental and stress parameters were comparable across animals.

DISCUSSION

In this study, we investigated the relationship between the CRF and its contacts on DA versus non-DA neurons in the PBP and A8 regions. These DA subregions were investigated since they are evolutionarily expanded in nonhuman primates (Halliday and Tork, 1986; McRitchie et al., 1996; Francois et al., 1999; Fu et al., 2016). The PBP and A8 have wide-ranging efferents beyond the those from the midline VTA (Williams and Goldman-Rakic, 1998; Francois et al., 1999; Haber et al., 2000; Fudge et al., 2017), and are also a site of intense CRF-immunoreactive fiber termination (**Figure 1**). We found that (1) CRF-positive axons terminated onto both DA positive and non-DA positive neurons in the PBP and A8 DA subregions; (2) CRF-positive axons formed both asymmetric and symmetric contacts, with a higher frequency of symmetric contacts in both PBP and A8; (3) In the PBP, significantly more CRF contacts were made onto non-DA neurons compared to DA neurons, however, the proportion of each synapse type did not significantly differ between cell types; (4) In A8, CRF contacts also made significantly more contacts on non-DA compared to DA neurons; significantly more CRF contacts on to non-DA were symmetrical (inhibitory); (5) same age male and female subjects had similar findings on all measures. Together these data suggest that CRF is a co-regulator of GABA and glutamate terminals in the PBP and A8, which largely influence non-DA neurons.

Comparison with previous work: CRF modulation of DA subcircuits

CRF fibers originate from multiple potential afferent sources to innervate the DA system (reviewed in, Kelly and Fudge, 2018). Our light microscopic results are consistent with previous studies using CRF immunostaining in monkey, and show that CRF-containing terminals overlap not only the midline VTA but also densely overlap the PBP and A8 regions (Foote and Cha, 1988). The specific sources of CRF to each of these regions remains to be determined.

Surprisingly, only one study has examined CRF expression in excitatory and inhibitory synapses in the VTA (Tagliaferro and Morales, 2008). In that rodent study, which broadly examined all VTA subnuclei (including the PBP), the majority (58%) of CRF-IR axon terminals targeted non-DA cells, and were predominantly symmetric (inhibitory) and thus, GABAergic in nature. We found, similarly, that the majority of CRF-positive contacts were onto non-DA cells in the monkey PBP and A8 (**Figure 4**). These contacts

bioRxiv preprint doi: https://doi.org/10.1101/2022.04.26.489587; this version posted April 28, 2022. The copyright holder for this preprint (which was not certified by peer review) is the author/funder. All rights reserved. No reuse allowed without permission.

were also predominantly symmetric with a significant bias towards enhanced inhibitory tone in the A8. In contrast to the Tagliaferro study, however, we did not find a preponderance of excitatory-type CRF profiles on DA neurons in either the PBP or A8. In fact, the overall number of CRF-containing terminals onto DA neurons were relatively small in both PBP and A8. Together, our results suggest that CRF is mainly expressed in GABAergic terminals, that largely contact non-DA neurons. We did not determine the phenotype of non-TH neurons but hypothesize that they are mostly GABAergic. While glutamatergic neurons also exist in the ventral midbrain, they are not a majority subpopulation (Nair-Roberts et al., 2008; Margolis et al., 2012; Yamaguchi et al., 2013; Root et al., 2016). In marmoset and human, glutamatergic neurons are highest in the rostrolinear nucleus of the midline VTA group, but drop off substantially in other subregions of the ventral midbrain. We thus hypothesize that the net effect of CRF/GABA synapses under basal conditions in the PBP and A8 is inhibition of post-synaptic GABAergic interneurons, which can release DA from inhibitory control in specific output paths (**Figure 7**).

During stress exposure in rodents, CRF is released into the VTA in an activity dependent manner (Wang et al., 2005). Electrophysiological studies demonstrate that CRF's postsynaptic effects on DA neurons can be inhibitory (Beckstead et al., 2009) or excitatory (Ungless et al., 2003; Wanat et al., 2008), and appear to be pathway specific. Thus, CRF can selectively gate afferent inputs to the VTA to re-prioritize motivated behavior (Wanat et al., 2013). For example, following anxiogenic and fear-provoking stimuli, GABAergic cells in the central nucleus of the amygdala (CeN) respond differentially based on the co-compartmentalized neuropeptide. Under non-stress (basal) conditions, GABA limits baseline anxiety, while CRF has little effect. However, chemogenetic manipulation of CRF-expressing GABA neurons in the CeN during fear learning shows that CRF is critical for enhancing fear acquisition (Pomrenze et al., 2019). These findings are consistent with the idea that CRF serves as a behavioral amplifier under stressful conditions by enhancing the action of the primary transmitter on post-synaptic neurons. Our results show that CRF terminals from all sources in the PBP and A8 mainly form inhibitory-type synapses onto non-DA (presumptive GABAergic) neurons. This organization suggests that CRF may have a regulatory ability in basal conditions but act to enhance DA signaling in stressful situations.

Balance of DA and GABA neurons across PBP and A8: implications for synaptic data

An important consideration in assessing quantitative data on CRF terminals pertains to the difference in ratios of TH:GAD post-synaptic partners in each region. GABAergic neurons comprise the largest non-dopaminergic cell population in the ventral midbrain (Nair-Roberts et al., 2008; Margolis et al., 2012), and contribute to potential modulation of local (and possible long-range) DA circuits (Carr and Sesack, 2000; Omelchenko and Sesack, 2009). In monkey, the ratio of DA to non-DA cells varies across the A10, A9 and A8 groups, and differs from the ratios in rodents (Swanson, 1982; Poirier et al., 1983; German and Manaye, 1993; Nair-Roberts et al., 2008). We recently quantified the distribution of DA neurons and their GABAergic counterparts throughout A10 (midline VTA and PBP separately), A9 (SNc) and A8 (RRF)

bioRxiv preprint doi: https://doi.org/10.1101/2022.04.26.489587; this version posted April 28, 2022. The copyright holder for this preprint (which was not certified by peer review) is the author/funder. All rights reserved. No reuse allowed without permission.

subregions in this cohort using unbiased stereology (Kelly et al. 2022, *under review*), and found significant regional differences in the balance of DA and GABAergic neurons. While there was an overall 3-fold greater number of DA neurons compared to GABAergic neurons, sub-regional ratios varied widely. The PBP has almost 5 times more DA neurons than GABAergic neurons; in contrast, in the A8 region, the ratio is close to 1:1. Here, we find that CRF fibers predominantly targeted non-DA (presumptive GABAergic neurons) in both PBP and A8, forming symmetric (inhibitory) contacts. Under our random sampling technique, there was an equal probability of finding a CRF contact on a DA versus non-DA cell. However, in the PBP, where DA neurons outnumbered GABA neurons by 5:1, there presumably was a smaller probability of finding CRF-non-DA contacts. Therefore, we suspect that in the PBP, we may be underestimating non-DA/CRF fiber interactions. In the A8 region, where GABA and DA neuron ratios are 1:1, estimates of CRF contacts are likely more accurate.

Beyond the classic VTA

DA is a key player in modulating diverse functions through specific input/output pathways. While initially viewed as a 'syncytium' (or mass) of cells, the midbrain DA system is now recognized to be highly heterogeneous with respect to both circuits and function. Early primate studies--in conjunction with findings in humans-- first hinted that the midbrain DA system must be differentially regulated by interdependent input/output channels (Brown et al., 1979; Davis et al., 1991). Elegant models in rodents now support this view, showing that the adjacent regions of the VTA are differentially involved in circuits and selective behaviors (Menegas et al., 2018; de Jong et al., 2019; Steinberg et al., 2020). The ways that different forms of stress affect specific DA subcircuits is a relatively new frontier (Douma and de Kloet, 2020; Verharen et al., 2020; Kong and Zweifel, 2021).

In rodents, the VTA receives CRF-containing afferents from lateral bed nucleus of stria terminalis (BSTL), the central nucleus of the amygdala (CeN), and the paraventricular nucleus (PVN) (Rodaros et al., 2007; Dabrowska et al., 2016). However, the CRF innervation of other DA subregions has generally been ignored. Dabrowska et al. (2016) recently used genetic approaches in mice and rats to show that CRF-synthesizing cells in the BSTL send relatively more intense fiber labeling over the substantia nigra pars compacta compared to the VTA. To examine the situation in non-human primates, we recently investigated inputs from the BSTL and CeN to the ventral midbrain in the monkey, and also found a relatively dense input *outside* the midline VTA subregion, i.e. to the PBP and A8. When examined with double-immunofluorescent experiments, retrograde tracer injections placed in the PBP and A8 DA subregions showed that a majority of labeled cells in the BSTL and CeN that co-contained CRF (Fudge et al., 2017).

On the output side, DA subregions that receive CRF inputs from the CeN--i.e. the PBP and A8-- project differentially to the striatum, compared to DA subregions that do not receive this input, such as the A9

bioRxiv preprint doi: https://doi.org/10.1101/2022.04.26.489587; this version posted April 28, 2022. The copyright holder for this preprint (which was not certified by peer review) is the author/funder. All rights reserved. No reuse allowed without permission.

(Fudge et al., 2017). The midline VTA in monkey, which also receives CRF inputs, likely receives the majority of these from other afferent sources. The midline VTA subnuclei and expanded PBP in monkey have distinct, interconnected input/output paths, suggesting that these A10 regions are distinct but in communication (Haber et al., 2000). In recent studies, further differences are being brought to light in DA projection patterns in the VTA in rodents that affect behavioral responses. These findings highlight that DA neurons in the medial versus 'lateral' VTA may indeed display differential projections and responses to 'emotional cues' (Lammel et al., 2011; Chaudhury et al., 2013; Beier et al., 2015). It is likely that evolutionary expansion of the ventral midbrain in primates results in differential efferent targets in DA neuron subregions and afferent targets in the striatum and cortex (reviewed in, Bjorklund and Dunnett, 2007; Cho and Fudge, 2010; Fudge et al., 2017). These studies support the importance for species comparisons to translate the effects of stress circuitry to human studies.

REFERENCES

Arias-Carrion O, Stamelou M, Murillo-Rodriguez E, Menendez-Gonzalez M, Poppel E (2010) Dopaminergic reward system: A short integrative review. Int Arch Med 3:24.

Arsenault MY, Parent A, Seguela P, Descarries L (1988) Distribution and morphological characteristics of dopamine-immunoreactive neurons in the midbrain of the squirrel monkey (saimiri sciureus). J Comp Neurol 267:489-506.

Bangasser DA, Valentino RJ (2012) Sex differences in molecular and cellular substrates of stress. Cell Mol Neurobiol 32:709-723.

Bangasser DA et al. (2013) Increased vulnerability of the brain norepinephrine system of females to corticotropin-releasing factor overexpression. Mol Psychiatry 18:166-173.

Beckstead MJ, Gantz SC, Ford CP, Stenzel-Poore MP, Phillips PE, Mark GP, Williams JT (2009) Crf enhancement of girk channel-mediated transmission in dopamine neurons. Neuropsychopharmacology 34:1926-1935.

Beier KT et al. (2015) Circuit architecture of vta dopamine neurons revealed by systematic input-output mapping. Cell 162:622-634.

Bjorklund A, Dunnett SB (2007) Dopamine neuron systems in the brain: An update. Trends Neurosci 30:194-202.

Bouvier D et al. (2008) Pre-synaptic and post-synaptic localization of epha4 and ephb2 in adult mouse forebrain. J Neurochem 106:682-695.

Bromberg-Martin ES, Matsumoto M, Hikosaka O (2010) Dopamine in motivational control: Rewarding, aversive, and alerting. Neuron 68:815-834.

Brown RM, Crane AM, Goldman PS (1979) Regional distribution of monoamines in the cerebral cortex and subcortical structures of the rhesus monkey: Concentrations and in vivo synthesis rates. Brain Research 168:133-150.

Carr DB, Sesack SR (2000) Gaba-containing neurons in the rat ventral tegmental area project to the prefrontal cortex. Synapse 38:114-123.

Chaudhury D et al. (2013) Rapid regulation of depression-related behaviours by control of midbrain dopamine neurons. Nature 493:532-536.

Cho YT, Fudge JL (2010) Heterogeneous dopamine populations project to specific subregions of the primate amygdala. Neuroscience 165:1501-1518.

Coco ML, Kuhn CM, Ely TD, Kilts CD (1992) Selective activation of mesoamygdaloid dopamine neurons by conditioned stress: Attenuation by diazepam. Brain Research 590:39-47.

Cote P-Y, Sadikot AF, Parent A (1991) Complementary distribution of calbindin d-28k and parvalbumin in the basal forebrain and midbrain of the squirrel monkey. European Journal of Neuroscience 3:1316-1329.

bioRxiv preprint doi: https://doi.org/10.1101/2022.04.26.489587; this version posted April 28, 2022. The copyright holder for this preprint (which was not certified by peer review) is the author/funder. All rights reserved. No reuse allowed without permission.

Dabrowska J, Martinon D, Moaddab M, Rainnie DG (2016) Targeting corticotropin-releasing factor (crf) projections from the oval nucleus of the bnst using cell-type specific neuronal tracing studies in mouse and rat brain. J Neuroendocrinol 10.1111/jne.12442.

Davis KL, Kahn RS, Ko G, Davidson M (1991) Dopamine in schizophrenia: A review and reconceptualization. Am J Psychiatry 148:11-10.

de Jong JW et al. (2019) A neural circuit mechanism for encoding aversive stimuli in the mesolimbic dopamine system. Neuron 101:133-151 e137.

Douma EH, de Kloet ER (2020) Stress-induced plasticity and functioning of ventral tegmental dopamine neurons. Neurosci Biobehav Rev 108:48-77.

Farassat N et al. (2019) In vivo functional diversity of midbrain dopamine neurons within identified axonal projections. Elife 8.

Foote SL, Cha CI (1988) Distribution of corticotropin-releasing-factor-like immunoreactivity in brainstem of two monkey species (saimiri sciureus and macaca fascicularis): An immunohistochemical study. J Comp Neurol 276:239-264.

Francois C, Yelnik J, Tande D, Agid Y, Hirsch EC (1999) Dopaminergic cell group a8 in the monkey: Anatomical organization and projections to the striatum. Journal of Comparative Neurology 414:334-347.

Fu Y, Paxinos G, Watson C, Halliday GM (2016) The substantia nigra and ventral tegmental dopaminergic neurons from development to degeneration. J Chem Neuroanat 76:98-107.

Fudge JL, Kelly EA, Pal R, Bedont JL, Park L, Ho B (2017) Beyond the classic vta: Extended amygdala projections to da-striatal paths in the primate. Neuropsychopharmacology 42:1563-1576.

Gallagher JP, Orozco-Cabal LF, Liu J, Shinnick-Gallagher P (2008) Synaptic physiology of central crh system. Eur J Pharmacol 583:215-225.

Garcia JP, Keen KL, Kenealy BP, Seminara SB, Terasawa E (2018) Role of kisspeptin and neurokinin b signaling in male rhesus monkey puberty. Endocrinology 159:3048-3060.

Gaspar P, Heizmann CW, Kaas JH (1993) Calbindin d-28k in the dopaminergic mesocortical projection of a monkey (aotus trivirgatus). Brain Res 603:166-172.

Gaspar P et al. (1983) Tyrosine hydroxylase and methionine-enkephalin in the human mesencephalon. J Neurol Sci 58:247-267.

German DC, Manaye KF (1993) Midbrain dopaminergic neurons (nuclei a8,a9, and a10): Three-dimensional reconstruction in the rat. J Comp Neurol 331:297-309.

Grieder TE et al. (2014) Vta crf neurons mediate the aversive effects of nicotine withdrawal and promote intake escalation. Nat Neurosci 17:1751-1758.

Haber SN, Fudge JL (1997) The primate substantia nigra and vta: Integrative circuitry and function. Crit Rev Neurobiol 11(4):323-342.

Haber SN, Fudge JL, McFarland N (2000) Striatonigrostriatal pathways in primates form an ascending spiral from the shell to the dorsolateral striatum. J Neurosci 20:2369-2382.

Halliday GM, Tork I (1986) Comparative anatomy of the ventromedial mesencephalic tegmentum in the rat, cat, monkey and human. J Comp Neurol 252:423-445.

Izzo E, Sanna PP, Koob GF (2005) Impairment of dopaminergic system function after chronic treatment with corticotropin-releasing factor. Pharmacol Biochem Behav 81:701-708.

Kalivas PW, Duffy P, Latimer LG (1987) Neurochemical and behavioral effects of corticotropin-releasing factor in the ventral tegmental area of the rat. J Pharmacol Exp Ther 242:757-763.

Kelly EA, Fudge JL (2018) The neuroanatomic complexity of the crf and da systems and their interface: What we still don't know. Neurosci Biobehav Rev 10.1016/j.neubiorev.2018.04.014.

Kelly EA, Tremblay ME, Gahmberg CG, Tian L, Majewska AK (2014) Subcellular localization of intercellular adhesion molecule-5 (telencephalin) in the visual cortex is not developmentally regulated in the absence of matrix metalloproteinase-9. J Comp Neurol 522:676-688.

Kelly EA, Contraras JM, Duan A, Vassell R, Fudge JL (2022) Unbiased stereological estimates of dopaminergic and gabaergic neurons in the a10, a9 and a8 subpopulations in the young male macaque. Neuroscience Under Review.

Kenealy BP, Keen KL, Kapoor A, Terasawa E (2016) Neuroestradiol in the stalk median eminence of female rhesus macaques decreases in association with puberty onset. Endocrinology 157:70-76.

bioRxiv preprint doi: https://doi.org/10.1101/2022.04.26.489587; this version posted April 28, 2022. The copyright holder for this preprint (which was not certified by peer review) is the author/funder. All rights reserved. No reuse allowed without permission.

Kong MS, Zweifel LS (2021) Central amygdala circuits in valence and salience processing. Behav Brain Res 410:113355.
Lammel S, Lim BK, Malenka RC (2014) Reward and aversion in a heterogeneous midbrain dopamine system. Neuropharmacology 76 Pt B:351-359.
Lammel S, Ion DI, Roeper J, Malenka RC (2011) Projection-specific modulation of dopamine neuron synapses by aversive and rewarding stimuli. Neuron 70:855-862.
Lavoie B, Parent A (1991) Dopaminergic neurons expressing calbindin in normal and parkinsonian monkeys. Neuroreport 2, No. 10:601-604.
Lewis DA, Sesack SR (1997) Dopamine systems in the primate brain. In: Handbook of chemical neuroanatomy, vol. 13: The primate nervous system, part 1 (F.E. Bloom ABaTH, ed), pp 263-375: Elsevier Science B.V.
Margolis EB, Toy B, Himmels P, Morales M, Fields HL (2012) Identification of rat ventral tegmental area gabaergic neurons. PLoS One 7:e42365.
Matsumoto M, Hikosaka O (2009) Two types of dopamine neuron distinctly convey positive and negative motivational signals. Nature 459:837-841.
McRitchie DA, Halliday GM, Cartwright H (1995) Quantitative analysis of the variability of substantia nigra pigmented cell clusters in the human. Neuroscience 68:539-551.
McRitchie DA, Hardman CD, Halliday GM (1996) Cytoarchitectural distribution of calcium binding proteins in midbrain dopaminergic regions of rats and humans. Journal of Comparative Neurology 364:121-150.
Menegas W, Akiti K, Amo R, Uchida N, Watabe-Uchida M (2018) Dopamine neurons projecting to the posterior striatum reinforce avoidance of threatening stimuli. Nat Neurosci 21:1421-1430.
Mirenowicz J, Schultz W (1994) Importance of unpredictability for reward responses in primate dopamine neurons. J Neurophysiol 72:1024-1027.
Morales M, Margolis EB (2017) Ventral tegmental area: Cellular heterogeneity, connectivity and behaviour. Nat Rev Neurosci 18:73-85.
Nair-Roberts RG, Chatelain-Badie SD, Benson E, White-Cooper H, Bolam JP, Ungless MA (2008) Stereological estimates of dopaminergic, gabaergic and glutamatergic neurons in the ventral tegmental area, substantia nigra and retrorubral field in the rat. Neuroscience 152:1024-1031.
Olszewski J, Baxter D (2014) Cytoarchitecture of the human brainstem, 3rd, revised and extended Edition. Basel: Karger.
Omelchenko N, Sesack SR (2009) Ultrastructural analysis of local collaterals of rat ventral tegmental area neurons: Gaba phenotype and synapses onto dopamine and gaba cells. Synapse 63:895-906.
Orozco-Cabal L, Pollandt S, Liu J, Shinnick-Gallagher P, Gallagher JP (2006) Regulation of synaptic transmission by crf receptors. Rev Neurosci 17:279-307.
Pearson J, Goldstein M, Markey K, Brandeis L (1983) Human brainstem catecholamine neuronal anatomy as indicated by immunocytochemistry with antibodies to tyrosine hydroxylase. Neuroscience 8, No. 1:3-32.
Peters A, Palay SL, Webster Hd (1991) The fine structure of the nervous system : Neurons and their supporting cells, 3rd Edition. New York: Oxford University Press.
Plant TM, Terasawa, Ei, Witchel, Selma Feldman (2015) Puberty in non-human primates and man. 5 Physiological Control Systems and Governing Gonadal Function Fourth Edition:1487-1536.
Poirier LJ, Giguere M, Marchand R (1983) Comparative morphology of the substantia nigra and ventral tegmental area in the monkey, cat and rat. Brain Res Bull 11:371-397.
Pomrenze MB, Giovanetti SM, Maiya R, Gordon AG, Kreeger LJ, Messing RO (2019) Dissecting the roles of gaba and neuropeptides from rat central amygdala crf neurons in anxiety and fear learning. Cell Rep 29:13-21 e14.
Rincon-Cortes M, Grace AA (2017) Sex-dependent effects of stress on immobility behavior and vta dopamine neuron activity: Modulation by ketamine. Int J Neuropsychopharmacol 20:823-832.
Rodaros D, Caruana DA, Amir S, Stewart J (2007) Corticotropin-releasing factor projections from limbic forebrain and paraventricular nucleus of the hypothalamus to the region of the ventral tegmental area. Neuroscience 150:8-13.

bioRxiv preprint doi: https://doi.org/10.1101/2022.04.26.489587; this version posted April 28, 2022. The copyright holder for this preprint (which was not certified by peer review) is the author/funder. All rights reserved. No reuse allowed without permission.

Root DH et al. (2016) Glutamate neurons are intermixed with midbrain dopamine neurons in nonhuman primates and humans. Scientific Reports 6.

Steinberg EE et al. (2020) Amygdala-midbrain connections modulate appetitive and aversive learning. Neuron 10.1016/j.neuron.2020.03.016.

Swanson LW (1982) The projections of the ventral tegmental area and adjacent regions: A combined fluorescent retrograde tracer and immunofluorescence study in the rat. Brain Res Bull 9:321-353.

Tagliaferro P, Morales M (2008) Synapses between corticotropin-releasing factor-containing axon terminals and dopaminergic neurons in the ventral tegmental area are predominantly glutamatergic. J Comp Neurol 506:616-626.

Tobler PN, Dickinson A, Schultz W (2003) Coding of predicted reward omission by dopamine neurons in a conditioned inhibition paradigm. Journal of Neuroscience 23:10402-10410.

Tremblay ME, Riad M, Bouvier D, Murai KK, Pasquale EB, Descarries L, Doucet G (2007) Localization of epha4 in axon terminals and dendritic spines of adult rat hippocampus. J Comp Neurol 501:691-702.

Ungless MA, Singh V, Crowder TL, Yaka R, Ron D, Bonci A (2003) Corticotropin-releasing factor requires crf binding protein to potentiate nmda receptors via crf receptor 2 in dopamine neurons. Neuron 39:401-407.

Verharen JPH, Zhu Y, Lammel S (2020) Aversion hot spots in the dopamine system. Curr Opin Neurobiol 64:46-52.

Wanat MJ, Bonci A, Phillips PE (2013) Crf acts in the midbrain to attenuate accumbens dopamine release to rewards but not their predictors. Nat Neurosci 16:383-385.

Wanat MJ, Hopf FW, Stuber GD, Phillips PE, Bonci A (2008) Corticotropin-releasing factor increases mouse ventral tegmental area dopamine neuron firing through a protein kinase c-dependent enhancement of ih. J Physiol 586:2157-2170.

Wang B, Shaham Y, Zitzman D, Azari S, Wise RA, You ZB (2005) Cocaine experience establishes control of midbrain glutamate and dopamine by corticotropin-releasing factor: A role in stress-induced relapse to drug seeking. J Neurosci 25:5389-5396.

Watabe-Uchida M, Zhu L, Ogawa SK, Vamanrao A, Uchida N (2012) Whole-brain mapping of direct inputs to midbrain dopamine neurons. Neuron 74:858-873.

Williams SM, Goldman-Rakic PS (1998) Widespread origin of the primate mesofrontal dopamine system. Cerebral Cortex 8:321-345.

Yamaguchi T, Wang HL, Morales M (2013) Glutamate neurons in the substantia nigra compacta and retrorubral field. Eur J Neurosci 38:3602-3610.

Yuan Y et al. (2019) Reward inhibits paraventricular crh neurons to relieve stress. Curr Biol 29:1243-1251 e1244.

bioRxiv preprint doi: https://doi.org/10.1101/2022.04.26.489587; this version posted April 28, 2022. The copyright holder for this preprint (which was not certified by peer review) is the author/funder. All rights reserved. No reuse allowed without permission.

TABLES

Table 1.

Experimental Case

Case	Weight (kg)	Age (years)	Sex
J32	5.4	3.3	M
J38	3.5	3.3	M
J41	4.1	4.5	M
J55	3.5	2.9	F
J58	4.0	2.9	F
J59	3.1	3.1	F

bioRxiv preprint doi: https://doi.org/10.1101/2022.04.26.489587; this version posted April 28, 2022. The copyright holder for this preprint (which was not certified by peer review) is the author/funder. All rights reserved. No reuse allowed without permission.

Table 2.

Antibodies Used

Antigen	**Immunogen**	**Source**	**Characterization Reference**	**Working Dilution**
Corticotropin Releasing Factor (CRF) Host: Rabbit	Polyclonal antibody collected from rabbits immunized with a synthetic peptide as the immunogen. Species cross reactivity: human, mouse, rat.	Peninsula Laboratories, Inc. (Bachem Group) T-4037	*Journal of Comparative Neurology* antibody database ID #**AB-518252**	1:1,000
Tyrosine hydroxylase (TH) Host: Mouse	Monoclonal antibody, clone LNC1. Recognizes an epitope on the outside of the regulatory N-terminus. Species cross-reactivity: human, mouse, rat, chicken, frog, monkey, and vole.	Millipore, MAB318	*Journal of Comparative Neurology* antibody database ID #**AB-2201528**	1:10,000
Calbindin (CaBP) Host: Mouse	Monoclonal antibody, clone CB-955. Highly conserved 28kD calcium binding protein with broad tissue distribution. Species cross-reactivity: rat, bovine, guinea pig, human, mouse, canine, sheep, rabbit, feline, goat, pig.	Sigma, C9848	*Journal of Comparative Neurology* antibody database ID #**AB-476894**	1:10,000

bioRxiv preprint doi: https://doi.org/10.1101/2022.04.26.489587; this version posted April 28, 2022. The copyright holder for this preprint (which was not certified by peer review) is the author/funder. All rights reserved. No reuse allowed without permission.

Table 3.

Pubertal and stress hormone descriptions

HORMONE	ROLE	DESCRIPTION
Androstenedione	Male: Developmental	Precursor of testosterone and other androgens. In addition to functioning as an endogenous prohormone, androstenedione also has weak androgenic activity.
Testosterone	Male: Developmental	Primary sex hormone and anabolic steroid in males. Testosterone plays a key role in the development of male reproductive tissues such as testes and prostate, as well as promoting secondary sexual characteristics such as increased muscle and bone mass and the growth of body hair.
Dehyroepiandrosterone (DHEA)	Male: Developmental	Also known as *androstenolone*, is an endogenous steroid hormone precursor. It functions as a metabolic intermediate in the biosynthesis of the androgen and estrogen sex steroids both in the gonads and various other issue.
Progesterone (P4)	Female: Developmental	Endogenous steroid and proestrogen sex hormone involved in the menstrual cycle, pregnancy, and embryogenesis of humans and other species.
Estrone (E1)	Female: Developmental	Also spelled *oestrone*, is a steroid, a weak estrogen and a minor female sex hormone. It is one of three major endogenous estrogens, the others being estradiol and estriol.
Estradiol (E2)	Female: Developmental	Also spelled *oestradiol*, is an estrogen steroid hormone and the major female sex hormone. It is involved in the regulation of the estrous and menstrual female reproductive cycle. Estrodiol is responsible for the development and of female secondary sexual characteristics.
Cortisone	Stress Response	A pregnane (21-carbon) steroid hormone. A precursor to cortisol.
Cortisol	Stress Response	A steroid hormone, in the glucocorticoid class of hormones. It is released with a diurnal cycle and its release is increased in response to stress and low blood-glucose concentration.

bioRxiv preprint doi: https://doi.org/10.1101/2022.04.26.489587; this version posted April 28, 2022. The copyright holder for this preprint (which was not certified by peer review) is the author/funder. All rights reserved. No reuse allowed without permission.

FIGURE LEGENDS

Figure 1.

Overview of CaBP and CRF immunoreactivity in ventral midbrain. **(A)** Low magnification brightfield micrograph of the ventral midbrain rostrocentral level, immunostained for CaBP. CaBP-positive midline and PBP A10 neurons contrast with CaBP-negative SNc/A9 neurons, outlined with dotted line. **(B)** A neighboring section to panel A, immunoreacted for CRF, visualized with darkfield microscopy. **(C)** A higher magnification of boxed region in B showing patches of thin beaded CRF-positive fibers in a section of the PBP. **(D)** Low magnification brightfield micrograph of CaBP in the caudal ventral midbrain. CaBP-reactive cellular staining is found in DA neurons of the A10 and RRF/A8, and absent in SNc/A9 DA neurons. **(E)** A neighboring section to panel D, immunoreacted for CRF, seen under dark-field microscopy. Dense CRF labeled fibers course through the RRF/A8, seen under higher magnification in **F** (taken from boxed area in E). Scale bar in A,B,D,E= 1 mm; C,F= 250 um. *Abbreviations:* III, Third nerve; CRF, corticotropin releasing factor; CaBP, calbindin-28kD; IP, interpeduncular nucleus; cp, cerebral peduncle; scp, superior cerebellar peduncle; ml, medial lemniscus; SNr, substantia nigra reticulata; PBP, parabrachial pigmented nucleus; RN, red nucleus; VTA, ventral tegmental area.

Figure 2.

Single immunocytochemistry for CRF, CaBP and TH. Neighboring compartments immuno-stained with CRF, CaBP and TH to identify and block regions of interest (ROIs) for immuno-EM processing. Rostral adjacent compartments containing PBP (**A, C, E**) assessed for CRF, CaBP, and TH immunoreactivity, respectively. Adjacent caudal compartments containing A8 (**B, D, F**) were similarly used to identify regions. Fiducial markers such as fascicular bundles (of the 3rd nerve, medial lemniscus [ml]) and blood vessels (asterisks) were used align region of interest in EM section.

Figure 3.

Representative examples of CRF/TH dual immuno-peroxidase reactivity with EM. (**A**) EM micrograph at 30K magnification depicting multiple CRF immunoreactive (DAB) axon terminals. TH positive reactive dendrites are labeled with gold/silver enhancement showing highly specific and restricted labeling to dendritic structures. (**B-G**) 50% zoomed in examples of CRF/TH immunoreactivity. Note- in several examples, CRF positive axon terminals are seen near but not in contact with TH positive dendritic structures. CRF DAB visualization did not obstruct categorization of synapse type (determined by an accumulation of postsynaptic proteins [PSDs] on the postsynaptic cell). Here we found a prevalence of CRF positive axons making symmetric (inhibitory, white arrowhead) onto non-DA positive reactive elements. Examples of asymmetric (excitatory, black arrowhead) contacts onto either TH-positive or TH-negative post-synaptic structures are reported based on the presence of a PSD with obvious thickness. Scale bar in (A)= 1 micron, in (B-G)= 500 nm. *Abbreviations:* CRF, corticotropin releasing factor; TH,

bioRxiv preprint doi: https://doi.org/10.1101/2022.04.26.489587; this version posted April 28, 2022. The copyright holder for this preprint (which was not certified by peer review) is the author/funder. All rights reserved. No reuse allowed without permission.

tyrosine hydroxylase; at, axon terminal; de, dendrite; ma, myelinated axon; PBP, parabrachial pigmented nucleus.

Figure 4.

Quantification of the frequency of CRF positive axon contacts in PBP/A10 and RRF/A8. (**A**) Colorized electron micrograph depicting DAB filled CRF positive axon terminal contacts in the ventral midbrain of the macaque. TH positive dendrites (pink) were visualized with gold/silver enhancement (electron dense gold particles). Color key: pink= TH positive dendrites, yellow= TH- dendrites, green= presynaptic terminals, blue=spines. Abbreviations: a= astrocytes, CRF=corticotropin releasing factor, De= dendrite, TH= tyrosine hydroxiylase. (**B**) Quantification of all CRF positive axon contacts across cell type (DA vs non-DA) in the PBP and A8. Significantly more contacts were found on non-DA cells in both PBP and A8. Within cell-type comparisons were not significantly different. (**C**) Quantification of synapse type (asymmetric,[+], excitatory; symmetric,[-],inhibitory) in PBP and A8. Proportion comparisons showed significantly more symmetric synapses vs asymmetric synapses in both PBP and A8. (**D**) Quantification of the proportion of CRF positive axon contacts across both cell type (DA vs non-DA) and synapse type (asymmetric [+] vs symmetric [-]) in PBP/A10. Significantly more synapses (both asymmetric and symmetric) were found in non-DA positive cells. Within cell type comparisons were not significantly different in synapse type. (**E**) Quantification of the proportion of CRF positive axon contacts across both cell type (DA vs non-DA) and synapse type (asymmetric [+] vs symmetric [-]) in RRF/A8. Significantly more synapses (both asymmetric and symmetric) were found in non-DA positive cells. Within cell type comparisons were not significantly different in synapse type in DA cells, however non-DA cells showed significantly more symmetric synapses. *Statistics:* Two-way ANOVA with corrected Tukey's multiple comparisons test. Significance based on $p \leq 0.05$. **= $p<0.005$, ***= $p<0.0001$.

Figure 5.

Quantification of CRF positive axon contacts in PBP/A10 and RRF/A8 in males vs females. (**A**) Comparison of CRF contacts onto DA versus non-DA neurons in males and females. For pooled data, there were significantly more CRF contacts on non-DA cells in the PBP and A8, with no differences between males and females. (**B**) Proportion of asymmetric [+] vs symmetric [-]) profiles in the PBP in males versus females was similar. (**C**) Proportion of asymmetric [+] vs symmetric [-]) profiles in the A8 in males versus females was similar with respect to relative contacts onto DA versus non-DA neurons. The proportion of asymmetric synapses on non-DA and DA cells was significantly greater for females; in males asymmetric synapses were significantly greater onto non-DA cells, but not onto DA cells (solid bars vs hatched bars; male: blue, female: red). Significantly more symmetric synapses were found in non-DA cells in both males and females. Within the non-DA cell populations, there were significantly more symmetric synapses in both sexes (male: blue comparison bar below graph, female: red comparison bar below

bioRxiv preprint doi: https://doi.org/10.1101/2022.04.26.489587; this version posted April 28, 2022. The copyright holder for this preprint (which was not certified by peer review) is the author/funder. All rights reserved. No reuse allowed without permission.

graph). *Statistics:* Two-way ANOVA with corrected Tukey's multiple comparisons test. Significance based on p≤ 0.05. *=p<0.05, **=P<0.005, ***=p<0.0001.

Figure 6.

Pubertal and stress hormone assays in adolescent male and female macaques. Gender-specific developmental hormones and stress hormone concentrations from serum in 7 male and female macaques. Male hormones: androstenedione, testosterone, and DHEA (brown, orange, blue); Female hormones progesterone, estrone and estradiol (yellow, green, blue). Stress hormones: cortisone and cortisol (pink, purple). Descriptions of hormones can be found in **Table 3.**

Figure 7.

Hypothesis of indirect CRF modulation of DA cells. CRF-positive axons predominantly make symmetric (inhibitory) contacts onto non-DA cells in both PBP and A8. We hypothesize that under stress, CRF in inhibitory contacts may enhance GABA effects on non-DA cells (presumptive GABA interneurons), resulting in a disinhibition of DA neurons.

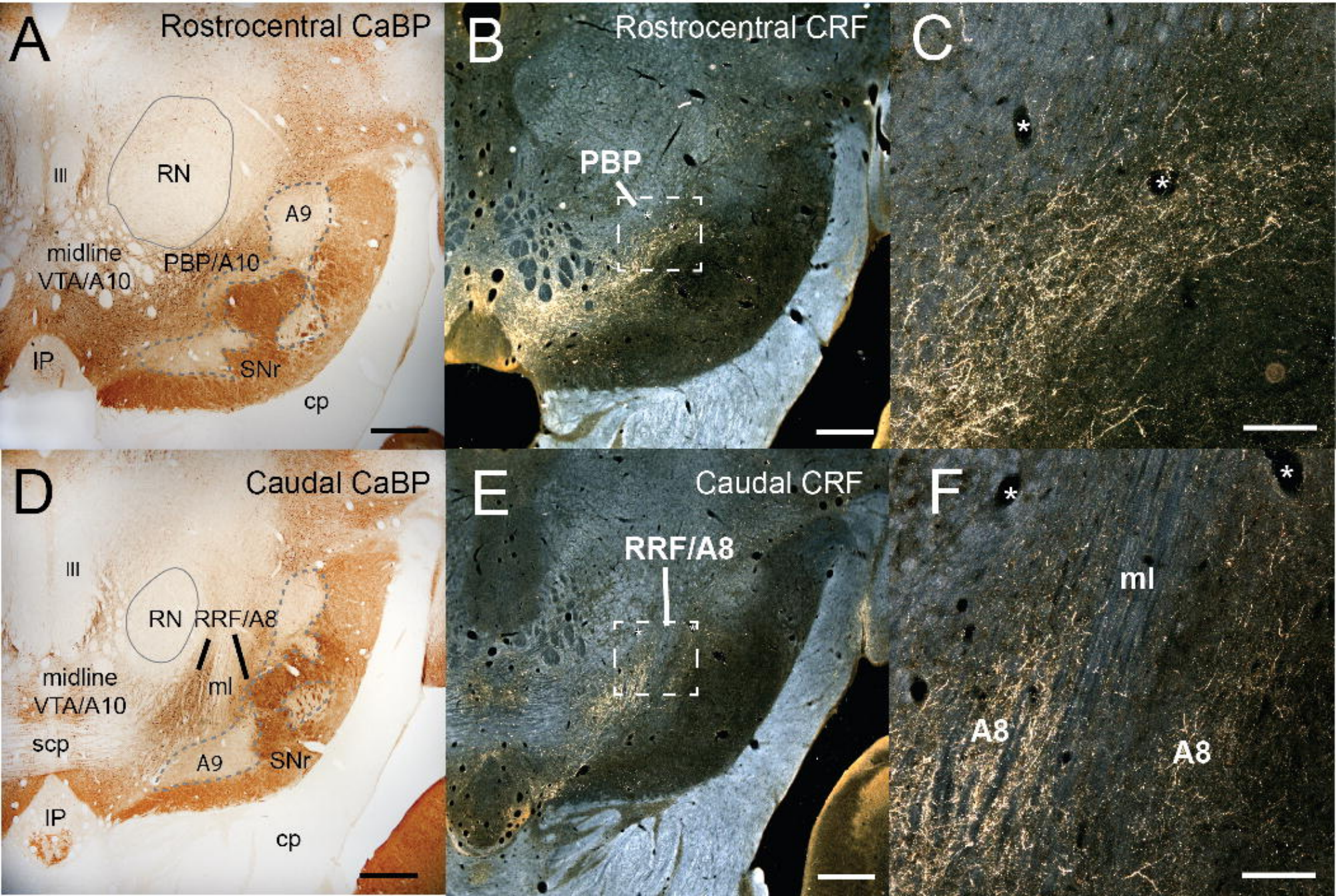
A
Rostrocentral CaBP
III
RN
A9
midline
VTA/A10
PBP/A10
IP
SNr
cp
B
Rostrocentral CRF
PBP
C
*
*
D
Caudal CaBP
III
RN
RRF/A8
midline
VTA/A10
ml
scp
A9
SNr
IP
cp
E
Caudal CRF
RRF/A8
F
*
*
ml
A8
A8

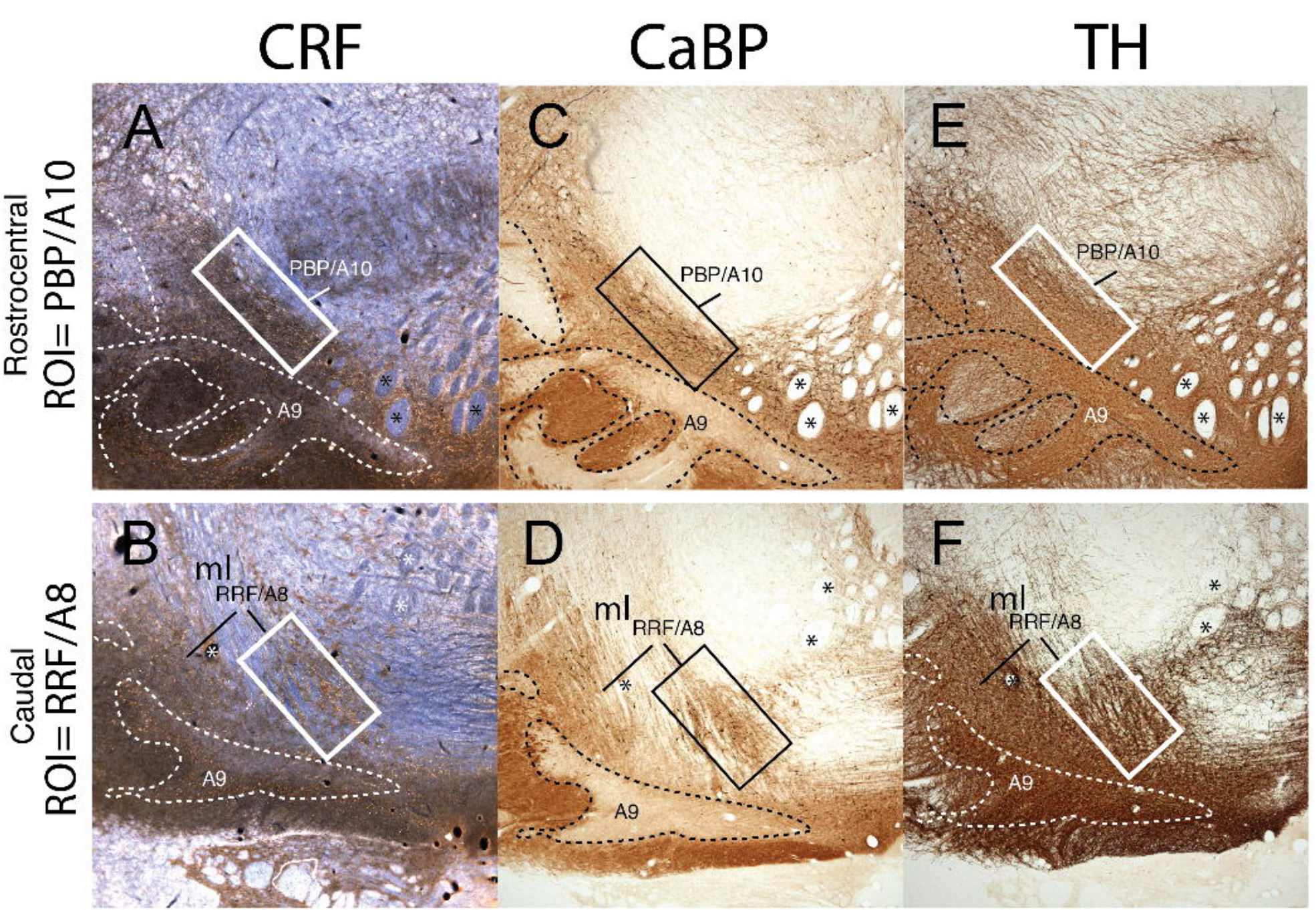
CRF
CaBP
TH
Rostrocentral
ROI= PBP/A10
Caudal
ROI= RRF/A8
A
C
E
B
D
F
PBP/A10
RRF/A8
ml
A9

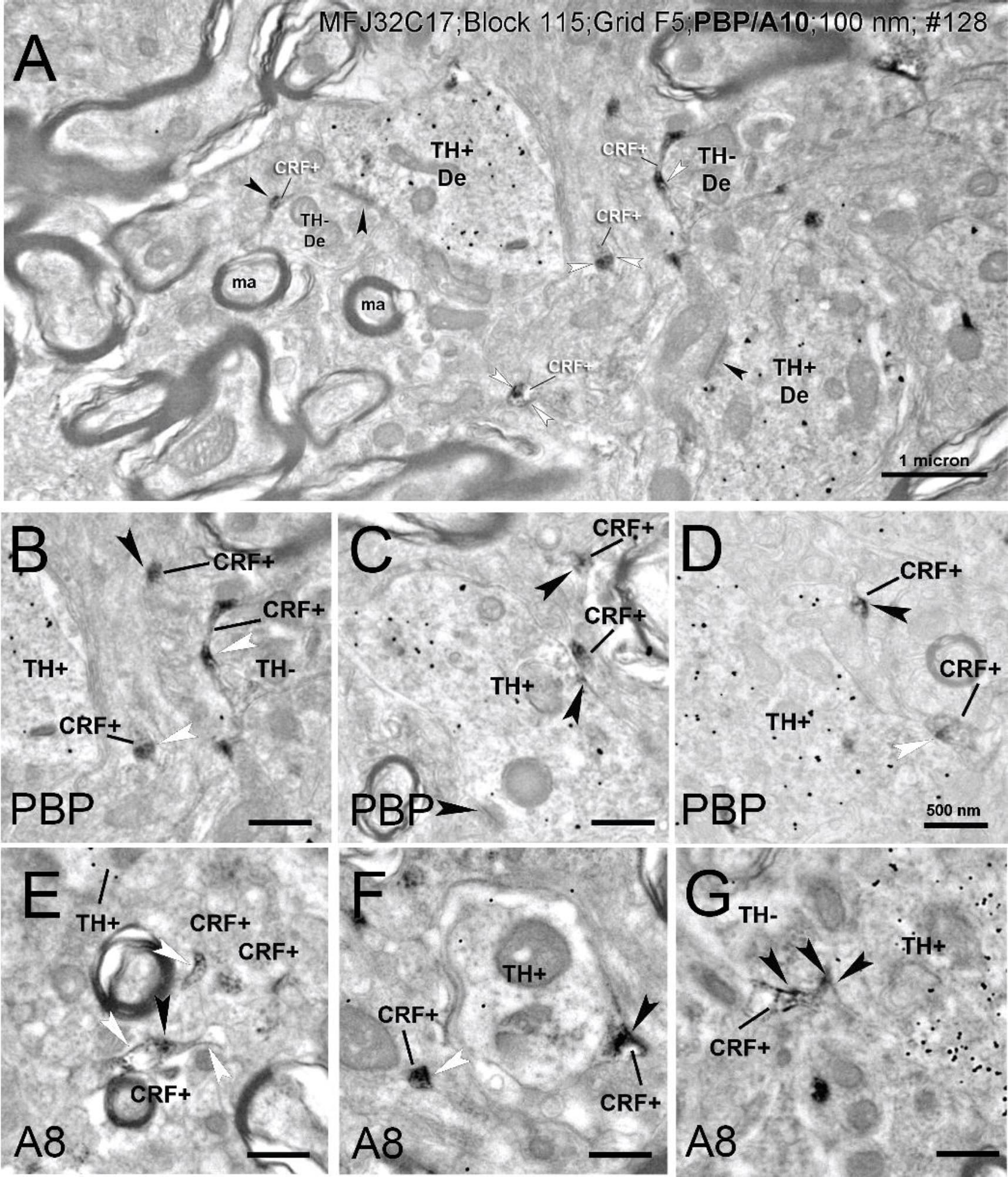
MFJ32C17;Block 115;Grid F5;PBP/A10;100 nm; #128
A
CRF+
TH+
De
TH-
De
ma
ma
CRF+
TH-
De
CRF+
CRF+
TH+
De
1 micron
B
CRF+
CRF+
TH+
TH-
CRF+
PBP
C
CRF+
CRF+
TH+
PBP
D
CRF+
CRF+
TH+
PBP
500 nm
E
TH+
CRF+
CRF+
CRF+
A8
F
TH+
CRF+
CRF+
A8
G
TH-
TH+
CRF+
A8

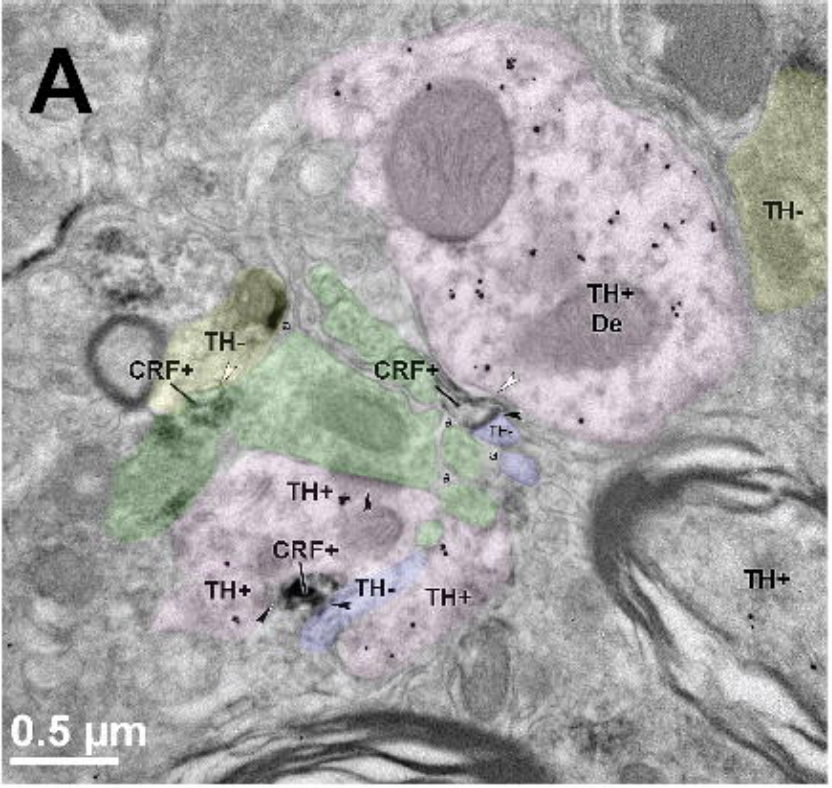
A
TH-
TH+
De
TH-
CRF+
CRF+
TH-
TH+
CRF+
TH+
TH-
TH+
TH+
0.5 µm

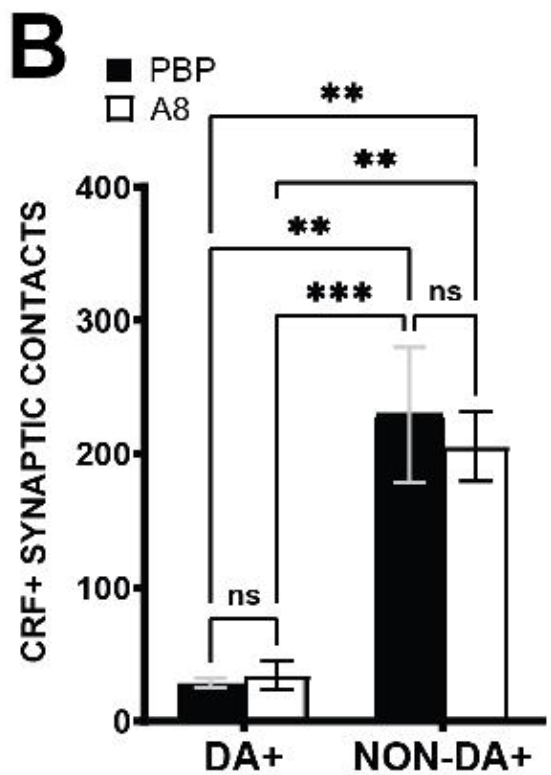
B
PBP
A8
CRF+ SYNAPTIC CONTACTS
400
300
200
100
0
**
**
**
***
ns
ns
DA+
NON-DA+

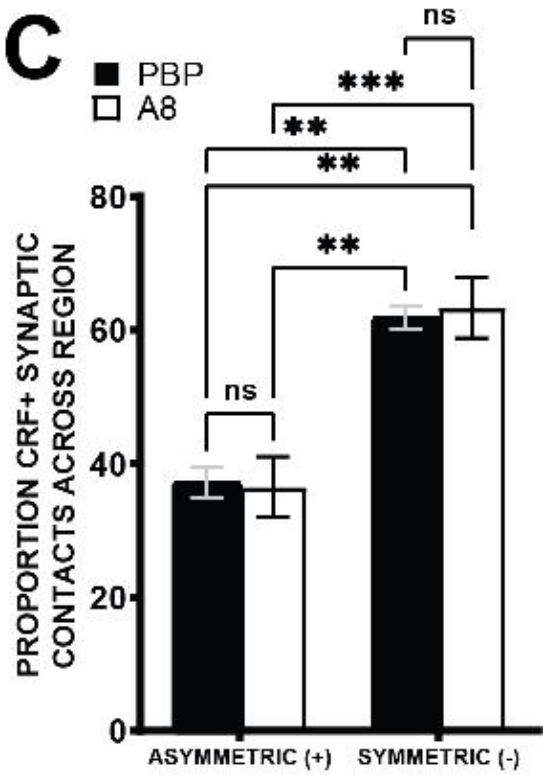
C
PBP
A8
PROPORTION CRF+ SYNAPTIC CONTACTS ACROSS REGION
80
60
40
20
0
ns
***
**
**
**
ns
ASYMMETRIC (+)
SYMMETRIC (-)

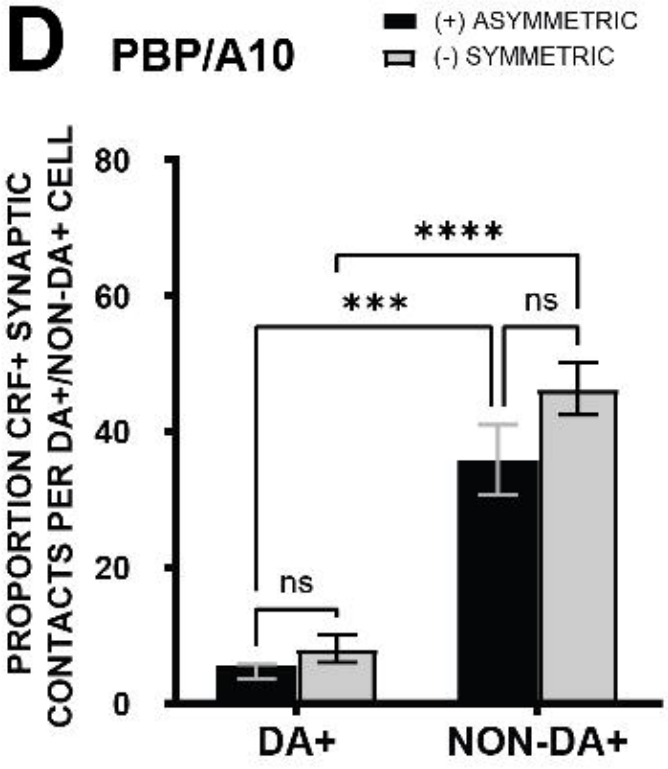
D
PBP/A10
(+) ASYMMETRIC
(-) SYMMETRIC
PROPORTION CRF+ SYNAPTIC CONTACTS PER DA+/NON-DA+ CELL
80
60
40
20
0
****
***
ns
ns
DA+
NON-DA+

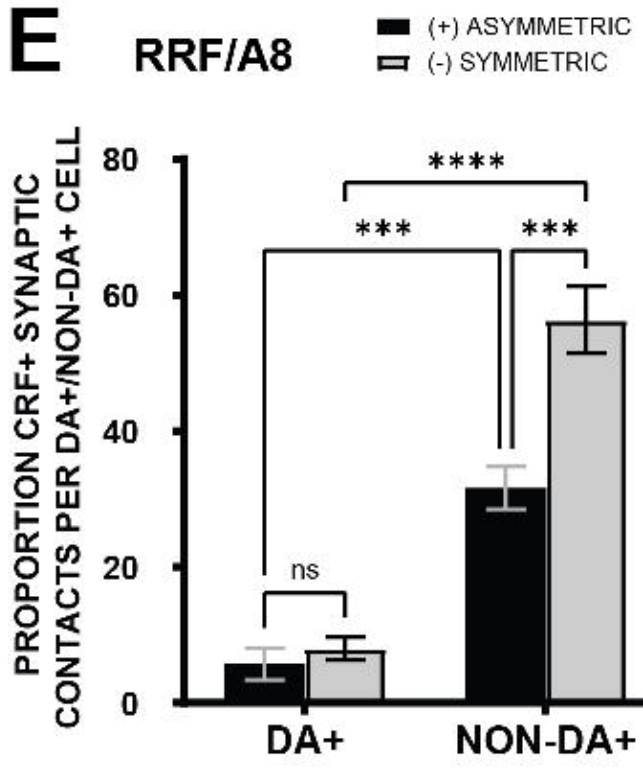
E
RRF/A8
(+) ASYMMETRIC
(-) SYMMETRIC
PROPORTION CRF+ SYNAPTIC CONTACTS PER DA+/NON-DA+ CELL
80
60
40
20
0
****
***
***
ns
DA+
NON-DA+

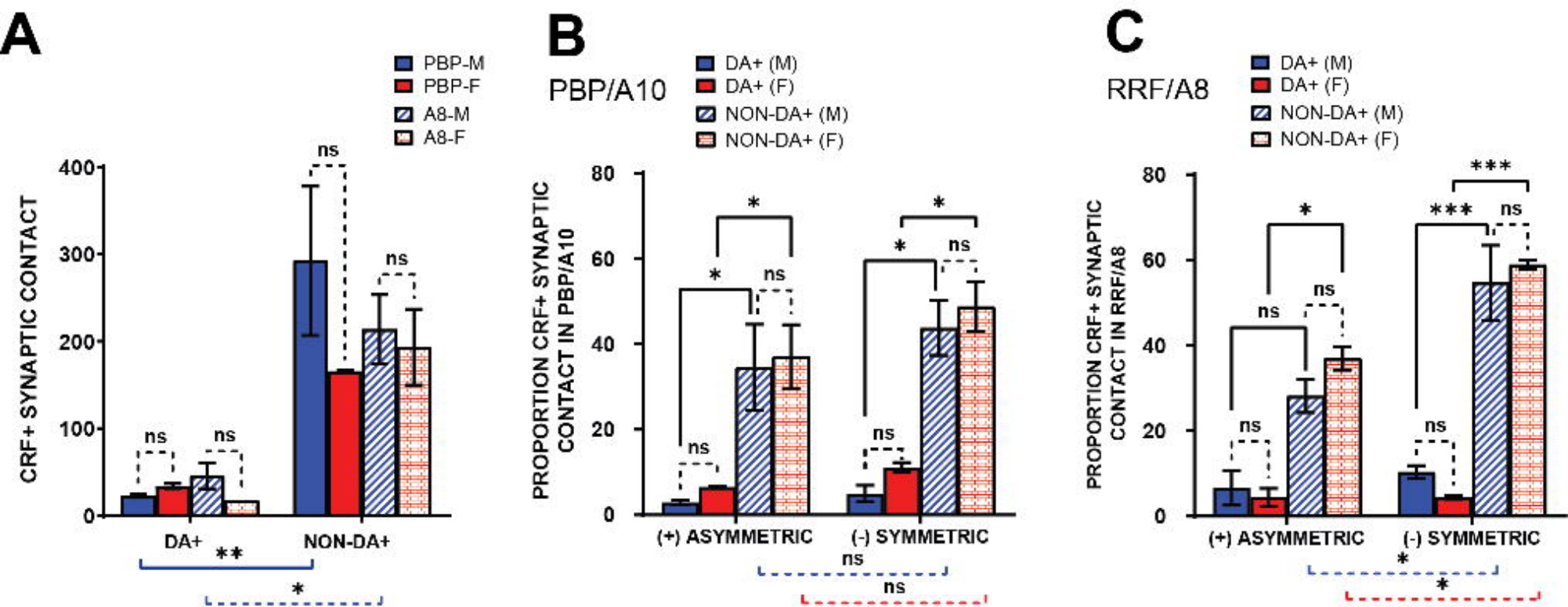
A
PBP-M
PBP-F
A8-M
A8-F
CRF+ SYNAPTIC CONTACT
400
300
200
100
0
ns
ns
ns
ns
DA+
NON-DA+
**
*
B
PBP/A10
DA+ (M)
DA+ (F)
NON-DA+ (M)
NON-DA+ (F)
PROPORTION CRF+ SYNAPTIC CONTACT IN PBP/A10
80
60
40
20
0
*
*
*
ns
*
ns
ns
ns
(+) ASYMMETRIC
(-) SYMMETRIC
ns
ns
C
RRF/A8
DA+ (M)
DA+ (F)
NON-DA+ (M)
NON-DA+ (F)
PROPORTION CRF+ SYNAPTIC CONTACT IN RRF/A8
80
60
40
20
0
***
*
***
ns
ns
ns
ns
(+) ASYMMETRIC
(-) SYMMETRIC
*
*

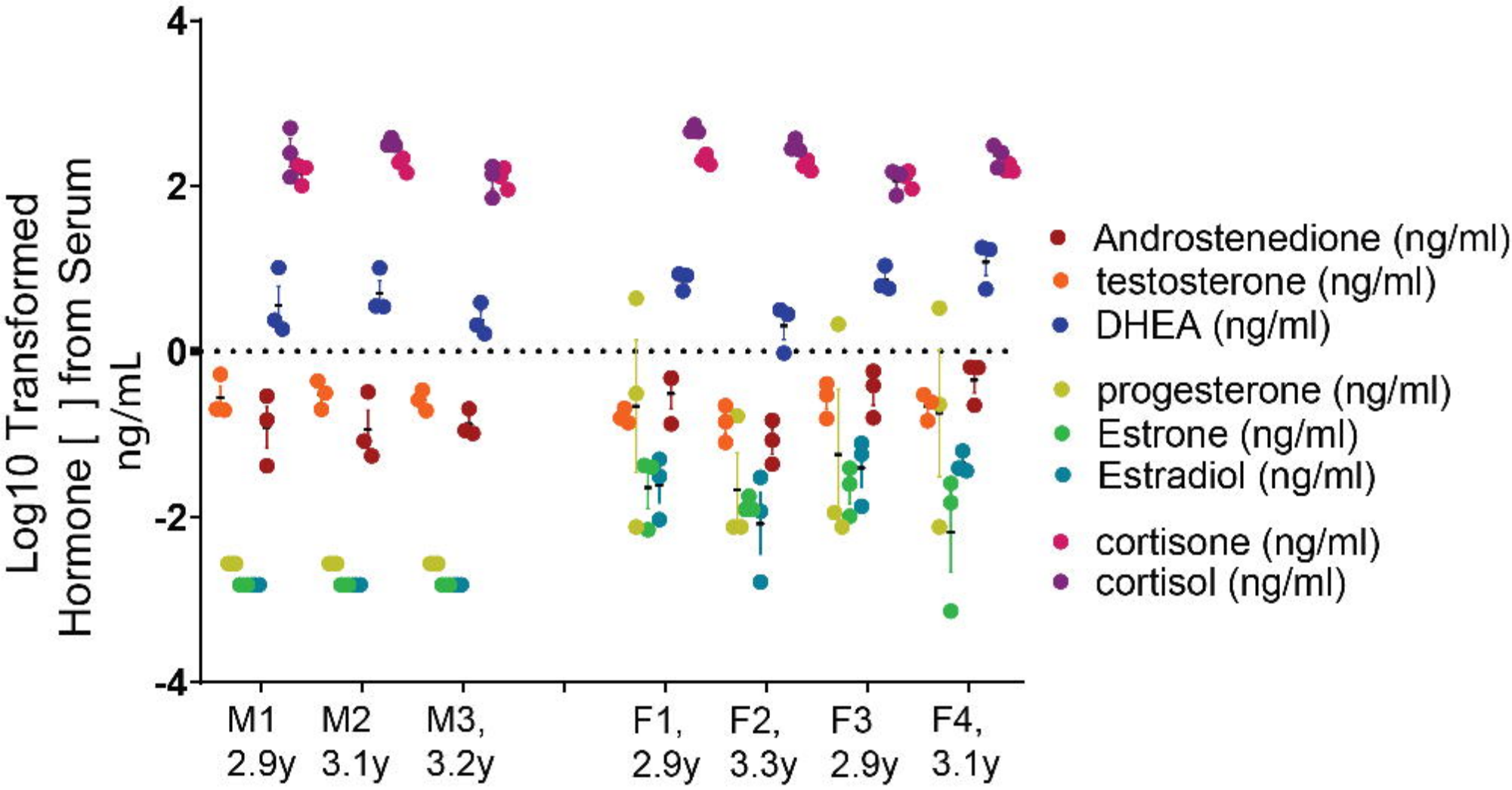
Log10 Transformed
Hormone [ ] from Serum
ng/mL
4
2
0
-2
-4
M1
2.9y
M2
3.1y
M3,
3.2y
F1,
2.9y
F2,
3.3y
F3
2.9y
F4,
3.1y
Androstenedione (ng/ml)
testosterone (ng/ml)
DHEA (ng/ml)
progesterone (ng/ml)
Estrone (ng/ml)
Estradiol (ng/ml)
cortisone (ng/ml)
cortisol (ng/ml)

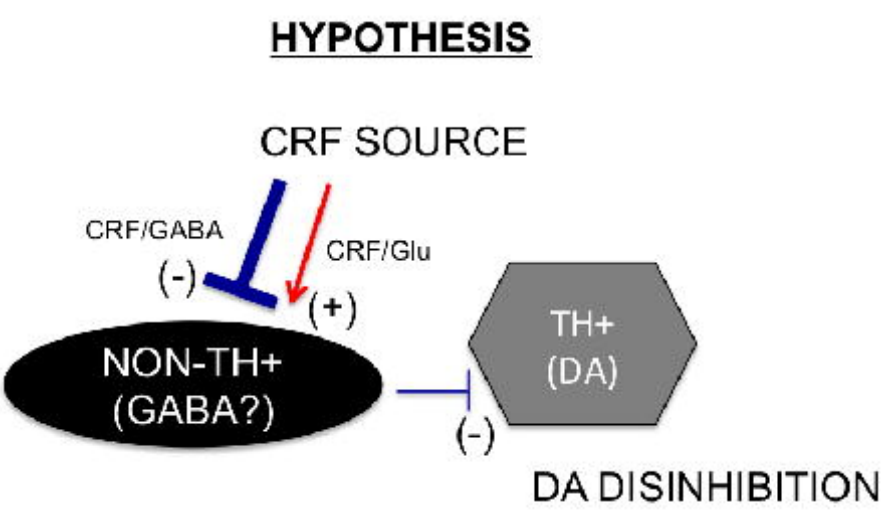
HYPOTHESIS
CRF SOURCE
CRF/GABA
(-)
CRF/Glu
(+)
NON-TH+
(GABA?)
TH+
(DA)
(-)
DA DISINHIBITION